# Clinical implementation of a portable primary-standard graphite calorimeter for absolute proton dosimetry in a low-energy passively scattered proton beam

A Lourenço[1,2], N Lee[1], D Shipley[1], F Romano[1,3], A Kacperek[4], S Duane[1], M Cashmore[1], G Bass[1], H Palmans[1,5] and R Thomas[1]

1 - Medical Radiation Science Group, National Physical Laboratory, Teddington TW11 0LW, United Kingdom
2 - Department of Medical Physics and Biomedical Engineering, University College London, London WC1E 6BT, United Kingdom
3 - Istituto Nazionale di Fisica Nucleare, Sezione di Catania, Via S Sofia 64, 95123, Catania, Italy
4 – The National Eye Proton Therapy Centre, The Clatterbridge Cancer Centre, Wirral CH63 4JY, United Kingdom
5 - Medical Physics Group, MedAustron Ion Therapy Center, A-2700 Wiener Neustadt, Austria

ana.lourenco@npl.co.uk

**Abstract**

Although calorimetry is the most direct way to measure absorbed dose, a calibration service based on a primary-standard calorimeter for the direct determination of absorbed dose for proton beams does not exist. A new Code of Practice for reference dosimetry of proton beams is being developed by a working party of the UK Institute of Physics and Engineering in Medicine (IPEM). The upcoming IPEM Code of Practice will recommend that users' ionisation chambers are calibrated directly in their clinical beams against the NPL proposed Primary-Standard Proton Calorimeter (PSPC) developed at the UK standards laboratory, the National Physical Laboratory (NPL). In this paper, user and NPL ionisation chambers were calibrated against the NPL PSPC in a low-energy passively scattered proton beam following recommendations of the upcoming IPEM Code of Practice. A comparison between the dose derived using the proposed IPEM Code of Practice and the IAEA TRS-398 protocol was performed. In total, 9 plane-parallel and 3 cylindrical chambers were calibrated using the two protocols for two separate visits. The ratio of absorbed dose to water obtained with the PSPC and dose to water obtained with ionisation chambers applying IAEA TRS-398 varied between 0.98 and 1.00, depending on the chamber type. The new procedure based on the NPL PSPC provides a significant improvement in uncertainty where absorbed dose to water measured with a user chamber is reported with an uncertainty of 0.9% at the 68% confidence level ($1\sigma$), whereas the IAEA TRS-398 protocol reports an uncertainty of 2.0% and 2.3% ($1\sigma$) for cylindrical and plane-parallel chambers, respectively. The establishment of a primary-standard calorimeter for the determination of absorbed dose in proton beams combined with the introduction of the associated calibration service following the IPEM recommendations will reduce the uncertainty and improve consistency in the dose delivered to patients.

## 1. Introduction

In the early 1970s, ICRU Report 24 (1976) recommended that the dose delivered to the planning target volume should be within 5% of the prescribed value at the 95% confidence level ($2\sigma$). The IAEA TRS-398 (2000) Code of Practice recognised this aim as unrealistic and rather a 5% uncertainty at the 68% confidence level ($1\sigma$) should be aimed, although for certain tumours a 3.3% or 3.5% ($1\sigma$) uncertainty would be more desirable. Nevertheless, these uncertainties are overall uncertainties and include dose delivery, dose measurement as well as dose calculation uncertainties, thus, in order to achieve them, reference absorbed dose-to-water measurements should be performed with an uncertainty below 1% ($1\sigma$) (Karger *et al.* 2010). For high-energy photons, the National Physical Laboratory (NPL), the UK's national measurement institute, provides calibrations based on a primary-standard calorimeter for the direct determination of absorbed dose to water with an uncertainty of 0.65% ($1\sigma$), which is in line with recommendations. A review of reference dosimetry audits performed over the last 20 years by the NPL for high-energy photons (Thomas *et al.* 2017) showed an improvement in the agreement of output ratios between NPL and the clinical facilities since the introduction of a single Code of Practice (Lillicrap *et al.* 1990) and associated calibration service (where calibrations were performed in a beam similar to that used clinically), as well as the use of a single dedicated secondary standard ionisation chamber type (the NPL 2611 and all previous versions NE 2611 and NE 2561). For reference dosimetry of proton beams, ICRU Report 78 (2008) recommends that the IAEA TRS-398 (2000) should be adopted for reference dosimetry. The IAEA TRS-398 recommends the use of ionisation chambers with a

calibration coefficient in terms of absorbed dose to water $N_{D,w,Q_0}$ in the reference calibration beam quality $Q_0$. Ideally, $Q_0$ should be the same as the user's beam quality, which, in this case, is a proton beam. However, as primary standards laboratories are not equipped with protons beams, IAEA TRS-398 recommends chambers to be calibrated in terms of absorbed dose to water in a $^{60}$Co beam and a beam quality correction factor $k_{Q,Q_0}$ is used to correct for differences between the ionisation chamber response in $^{60}$Co and that in a proton beam ($k_{Q,Q_0}$ is denoted as $k_Q$ when $Q_0$ is a $^{60}$Co beam). It is recommended (Andreo *et al.* 2000) that $k_Q$ values should be determined experimentally and be traceable to relevant primary standards. As such data were not available at that time for proton beams, IAEA TRS-398 provided $k_Q$ factors that are derived analytically for various ionisation chamber types.

Calorimetry is the most direct way to measure absorbed dose and several studies have reported the use of calorimeters in proton beams (Verhey *et al.* 1979, Schulz *et al.* 1992, Siebers *et al.* 1995, Palmans *et al.* 1996, Delacroix *et al.* 1997, Gagnebin *et al.* 2010, Palmans *et al.* 2004, Medin 2010, Sarfehnia *et al.* 2010, Renaud *et al.* 2016); however, a calibration service based on a primary standard calorimeter does not exist. Currently, NPL's absorbed dose standards are graphite calorimeters. These have been developed taking advantage of their sensitivity (the temperature rise in graphite is approximately six times that of water for the same dose) and thermal diffusivity, which is larger in graphite than in water (the heat dissipates quicker in graphite which allows more measurements to be completed within a similar timescale). A dedicated small-body portable graphite calorimeter was developed and tested by NPL in a clinical low-energy passively scattered proton beam (Palmans *et al.* 2004). They compared the dose measured with the small-body calorimeter and the dose obtained with ionisation chambers, calibrated at NPL in $^{60}$Co, using the IAEA TRS-398 for modulated and non-modulated proton beams. For the modulated beam, the dose ratio derived from the calorimeter and ionisation chambers applying the IAEA TRS-398 protocol varied from 0.98 to 1.01 while, for the non-modulated beam, it varied from 1.01 to 1.04 depending on the ionisation chamber type. Following the experience with this small-body calorimeter, NPL has built a Primary-Standard Proton Calorimeter (PSPC) for proton therapy beams.

A Working Party from the Institute of Physics and Engineering in Medicine (IPEM) is developing a Code of Practice for reference dosimetry of proton beams (Green *et al.* 2017). The IPEM Code of Practice will utilise the NPL proposed PSPC and it will enable the provision of a direct absorbed dose to water calibration in proton therapy centres with an uncertainty of 0.9% (at $1\sigma$). This is a considerable improvement as the IAEA TRS-398 reports an uncertainty of ≥2.0% ($1\sigma$) for the determination of absorbed dose to water in proton beams. The IPEM Code of Practice will recommend the use of the Roos-type plane-parallel chamber as the transfer and reference standards for proton beams. Definitive dose calibrations will be performed in the middle of the spread-out Bragg peak (SOBP) of a modulated beam (termed a standard test volume).

This work presents the application of the NPL proposed PSPC in a low-energy passively scattered proton beam following recommendations of the IPEM Code of Practice for proton beams. A comparison between the dose derived with the IAEA TRS-398 protocol and the upcoming IPEM Code of Practice is performed.

## 2. Materials and Methods

### *2.1. Measurements*

Measurements were performed at the 60 MeV ocular proton beam at the National Centre for Eye Proton Therapy, Clatterbridge Cancer Centre (CCC), UK. A brass collimator of 3 cm diameter was used with full-modulation (i.e., modulated from the surface to the distal edge) and the beam was setup to deliver 10 monitor units (MU) at a rate of 20 MU/min (about 0.78 Gy/MU). A transmission monitor ionisation chamber (PTW type 7862) was inserted in front of the nozzle as a precision beam monitor. Figure 1 shows the three experimental setups under consideration:

1. Setup 1: Ionisation chambers in a water phantom;
2. Setup 2: NPL PSPC;
3. Setup 3: Ionisation chambers in a graphite phantom.

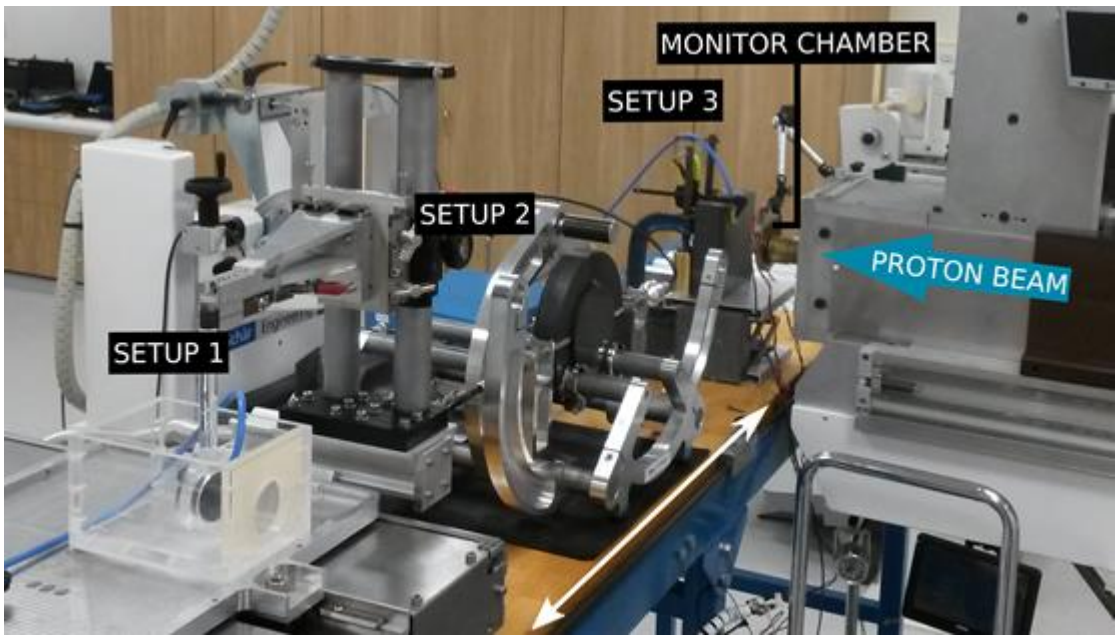


**Figure 1.** Experimental setups at CCC (the white arrow indicates that the table was on rollers which allows the three setups to be positioned sequentially in front of the beam).

The reference points of the ionisation chambers and calorimeter were positioned on the central axis of the beam at the isocentre and the source-to-detector (SDD) distance was kept constant. The reference point was positioned in the middle of the full-modulated beam at a water-equivalent depth of 1.56 g·cm$^{-2}$. The different experimental setups were placed on a moving platform at the correct height and SDD distance, which allowed for an easy transition between setups as shown in figure 1. Ionisation chamber and calorimeter measurements were performed on the same day to avoid day-to-day beam variations. Measurements were made on two consecutive days for each of two separate visits, one-year apart. One dataset of experiments consisted of (i) ionisation chamber measurements either in the water or graphite phantom (5 repeat readings of the standard to monitor ratio for each ionisation chamber operated at a specific voltage), (ii) at least 20 calorimeter runs at each mode of operation and (iii) a final ionisation chamber reading to check for consistency. These datasets were repeated throughout the two visits. On the first visit, two datasets of ionisation chamber measurements in graphite were repeated on the first day, while on the second day two datasets of ionisation chamber measurements in graphite and water, respectively, were performed. On the second visit, two datasets of ionisation chamber measurements in graphite and water were carried out on the first day, respectively, while on the second day one dataset of ionisation chamber measurements in water was performed.

*2.2. NPL PSPC*

*2.1.1. Calorimeter system.* The calorimeter has a nested construction which comprises disc shaped, and disc mantled graphite components, separated in a vacuum system to minimise heat transfer between components and the environment. The graphite calorimeter measures the temperature rise in the graphite core induced by absorption of ionising radiation. Changes in temperature are measured very accurately and precisely (considerably better than 100 μK) by small thermistors (0.8 mm long and 0.4 mm in diameter) embedded in each of the graphite components of the calorimeter. The core (nominally 2 mm thick and 16 mm in diameter) is enclosed within the inner and outer jackets which, in turn, are enclosed within a mantle. These components were manufactured in two parts named “front” and “back” for the jackets and “lid” and “base” for the mantle (see figure 2). Thermistors (manufactured by GE Sensing) are positioned equidistantly around the circumference of each component and embedded approximately 1.5 mm deep below the radial surface of each piece of graphite. The core contains two sensing thermistors and two heating thermistors, the inner and the outer jackets each contain four sensing and four heating thermistors, the mantle lid and the mantle base each contain two sensing thermistors.

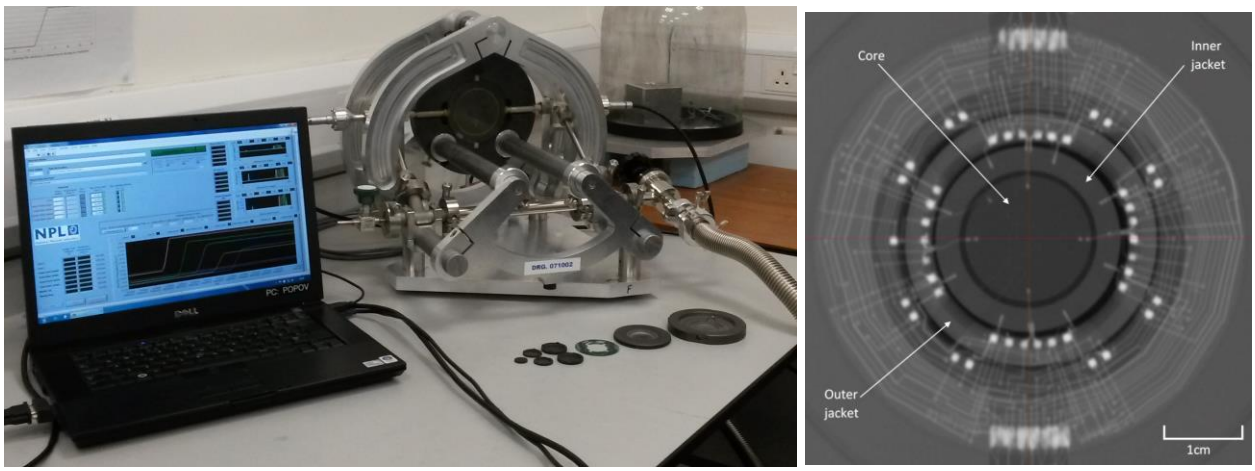


(a) (b)

**Figure 2.** (a) NPL PSPC with LabVIEW control program running. In front of the calorimeter, replicas of the different graphite components can be seen (left-right: core, front and back inner jackets, front and back outer jackets, PCB, mantle lid and mantle base). (b) Radiograph of the NPL PSPC which shows the thermistors embedded in the core, inner and outer jackets, and the connections to the radial PCB.

The wires (30 μm in diameter) from the thermistors are connected to a ring-shaped printed circuit board (PCB) positioned around the outer circumference of the inner jacket and sandwiched between the front and back parts of the outer jacket and mantle. The wires from the PCB connect to vacuum feed-through connectors to an interface box which, in turn, is connected to the measurement instrumentation that is controlled by a LabVIEW program. The two sensing thermistors in the core are independent of each other and connected to their own Wheatstone bridges while the sensing thermistors in each of the other components are connected into networks, each component network is connected to its own Wheatstone bridge. As with the sensing thermistors, the heating thermistors are electrically connected in a similar parallel network and the PCB in the calorimeter assists in the cable management between the various connections. Each thermistor network is connected via the interface box to one arm of separate DC Wheatstone bridges. The Wheatstone bridges consist of three 25 kΩ VH102Z Series Vishay high precision, hermetically sealed, metal foil resistors with provision to add further resistors in parallel to enable balancing of the Wheatstone bridge at different values of resistance and therefore temperature. The Wheatstone bridges currently balance at approximately 22 °C. The Wheatstone bridges are built into a chassis and all are powered by one bespoke-built 1.4 Volt high-stability direct current power supply unit. The sensing thermistors feed back to the measurement instrumentation controlled by a LabVIEW program, which controls the power supply to the heating thermistors and provide the required power to increase or decrease the temperature.

Independent control of each calorimeter component provides a flexible system and various possible modes of operation. In this work, calorimeter measurements were performed by operating the calorimeter in active isothermal and quasi-adiabatic irradiation modes (Seuntjens and Duane, 2009). For simplicity, active isothermal will be referred as isothermal and quasi-adiabatic irradiation will be referred as quasi-adiabatic. In isothermal mode, all components operate in constant temperature mode and the energy in the radiation beam is derived from the difference in electrical power required to maintain the core at a constant temperature before and then during the period the beam is incident on the core, i.e., by electrical substitution. In quasi-adiabatic mode, the outer-jacket is set to run in constant temperature mode whilst the inner-jacket and core run in constant power mode set to zero Watt. This provides a more stable environment for the core when carrying out adiabatic measurements of the radiation beam, i.e. when energy is derived from the measurement of the temperature rise of the core due to the radiation absorbed.

*2.2.2. Measurement equation and correction factors.* In this work, absorbed dose to water averaged over the disc area of the core $D_{w,Q}^{w,cal}$ per monitor unit (MU) at a reference depth $z_{ref}$ was obtained from the energy deposited in the core by ionising radiation $E_{core}^{rad}$ divided by the mass of the core $m_{core,eff}$, and the product of necessary correction factors ($k_i$),

$$\frac{D_{w,Q}^{w,cal}}{MU} = \frac{E_{core}^{rad}}{m_{core,eff}} . \prod k_i \qquad (1)$$

where $E_{core}^{rad}$ is equal to the total energy deposited in the core, minus the surplus energy dissipated by electrical power changes and energy received by heat transfer from calorimeter components (Seuntjens and Duane 2009),

$$E_{\text{core}}^{\text{rad}} = m_{\text{core,eff}} c_{\text{core}} \Delta T_{\text{core}} - \int \Delta P_{\text{core}} dt - \sum_j \int h_{\text{core},j} (T_j - T_{\text{core}}) dt \qquad (2)$$

$c_{\text{core}}$ is the average specific heat capacity of the core including all non-graphite materials and is defined as the total heat capacity of the core $C_{\text{core}}$ divided by its mass $m_{\text{core,eff}}$ and $\Delta T_{\text{core}}$ is the temperature rise in the core. The core is defined as all the materials that are located within the outline of the core and includes thermistors, epoxy and wires. The specific heat capacity of the core was calculated by considering the mass weighted sum of the specific heat capacities of the individual components. The second term is the energy from electrical heating of the core which is derived by integrating the increase in electrical power in the core over time. The third term is the energy received by heat transfer from calorimeter components $j$ to the core obtained by integration over time of the difference in temperature $T$ between the individual components and the core and a previously determined heat transfer coefficient $h_{\text{core},j}$. Heat transfers are inherently considered with fitting and extrapolating the pre-irradiation and post-irradiation temperature drift curves to account for the environmental temperature changes during irradiation. Temperature difference in the heat transfer term (equation 2, third term) are only relative to this temperature baseline. The following correction factors, $k_i$, are considered:

The impurity correction factor, $k_{\text{imp}}$, accounts for the radiological effect caused by the presence of the thermistors, epoxy and wires within the core. It is defined as the ratio of the average dose over the graphite core volume in a geometry of pure graphite with vacuum gaps present, and the average dose over the graphite core volume in the real geometry with all non-graphite components (Shipley *et al.* 2018). This correction is determined with Monte Carlo simulations performed with TOPAS code v3.6.p1 based on Geant4 v10.6.p01 (Perl *et al.* 2012).

$k_{\text{gap}}$ is the correction for the presence of vacuum gaps between the different components of the calorimeter. It is defined as the ratio of the average dose over the graphite core volume when the geometry is composed of homogenous graphite (that is, a compensated geometry with the vacuum gaps filled with graphite so that the same thickness of graphite remains in front of the core) and the average dose over the graphite core volume in the geometry with vacuum gaps; the so-called compensated gap approach (Shipley *et al.* 2018). This correction is determined with Monte Carlo simulations performed with TOPAS code v3.6.p1 based on Geant4 v10.6.p01 (Perl *et al.* 2012).

$k_{\text{z,cal}}$ is the correction factor for the reference distance from the beam. The decrease of absorbed dose with distance from the beam obeys the inverse square law.

$k_{\text{ripple}}$ is the correction factor for the degree of ripple in the flat region of the depth-dose distribution in which measurements are made. At CCC, the ripples on the modulated beam are due to the coarseness of the modulating wheel and have a period of about 1 mm and an amplitude of 0.25%. This correction is taken as unity with an associated uncertainty (see section 3.5.).

$s_{\text{w,g}} \cdot k_{\text{fl}}$ is the conversion from absorbed dose to graphite in a graphite phantom to absorbed dose to water in a water phantom at water-equivalent depths. It is defined as the product of the water-to-graphite mass-stopping-power ratio $s_{\text{w,g}}$ and the fluence correction factors $k_{\text{fl}}$ (Palmans *et al.* 2013, Lourenço *et al.* 2016). Monte Carlo simulations to account for this correction were performed with the FLUKA-2021.2.0 code (Ferrari et al 2005, Böhlen et al 2014).

Note that in equation 1, the quantity of interest is absorbed dose averaged over the core disc area. The graphite core was designed to have a similar diameter as the collecting volume of a Roos-type plane-parallel ionisation chamber, thus sampling a similar area of the beam.

For the simulations of the Monte Carlo derived corrections, the new recommendations by ICRU Report 90 (2016) for water and graphite $I$-values, $I_{\text{w}}$ = 78 eV and $I_{\text{g}}$ = 81 eV, respectively, were considered. In the Monte Carlo simulations, the full geometry of the CCC beam line was implemented (Bonnett *et al.* 1993, Baker *et al.* 2006, Kacperek 2009). To create a full-modulated beam in the Monte Carlo simulation, the individual beamlets were obtained by changing the thickness of the PMMA energy degrader. The weights of the individual beamlets were then optimized using a Matlab script (Romano *et al.* 2017) to achieve the required full-modulated beam.

For simulations performed with TOPAS, the default Modular physics list was selected which uses the reference hadronic physics list g4h-phy_QGSP_BIC_HP as well as the standard electromagnetic physics models (g4em-emstandard_opt4) with production cut-off of 0.05 mm for all particles.

For simulations with the FLUKA code, the default card HADROTHErapy was activated with the delta-ray production cut set to infinity as secondary electrons have short ranges and their energy was considered to be absorbed locally. Charged particle fluence differential in energy was scored in bins of 0.22 MeV and 0.007 cm in water and at scaled depths in graphite. The entire beamline was simulated; a collimator of 3 cm diameter was used, particle fluence was scored within a diameter equal to the calorimeter core and the measurement point in the water and graphite phantoms was positioned at the isocentre at water-equivalent depths. A total number of $500\times10^7$ primary protons were simulated.

*2.2.3. Calorimeter measurements and analysis method.* In this work, calorimeter measurements were performed by operating the calorimeter in isothermal and quasi-adiabatic modes. To position the core at the required water-equivalent depth, graphite build-up plates were added in front of the calorimeter. The water-equivalent thickness of the graphite build-up plates was determined experimentally by performing range measurements in water with and without the graphite plates in front of a water phantom (Lourenço *et al.* 2016). For a reference depth in water of 1.56 g·cm$^{-2}$, the equivalent graphite mass thickness was found to be 1.79 g·cm$^2$. For each calorimeter session, the irradiations were repeated at least 20 times to achieve a standard relative uncertainty (Type A) of 0.1% or better in the dose measured. Each calorimeter run is used to measure absorbed dose to graphite per monitor unit. The data is analysed using an in-house developed Matlab program where each calorimeter run is analysed independently. For each measurement, the radiation energy is determined from equation 2: (i) the total energy (determined from the measured temperature by the sensing thermistors), minus (ii) the energy from electrical heating (from the measured energy power by the heating thermistors), minus (iii) the energy gained by heat transfer from other calorimeter components to the core (from the measured temperature difference between calorimeter components) (Seuntjens and Duane 2009). The vacuum system between the different components limits the heat transfer through conduction and convection. The effect of unaccounted-for heat transfers is corrected by making a 4-parameter least squares fit of pre- and post- radiation energy to a common quadratic function of time (3 parameters), with an adjustable offset (the 4$^{th}$ parameter) between the pre- and post-irradiation drift curves. The ionising radiation energy absorbed by the core for each run is determined as the optimal value of this offset. This radiation energy is divided by the core mass to obtain the absorbed dose.

*2.3. Ionisation chambers and calibration procedures*

Ionisation chamber measurements were performed in a water phantom (figure 1, setup 1) and in a graphite phantom (figure 1, setup 3). Nine plane-parallel ionisation chambers (six PTW 34001 Roos – SN 711, 1684, 2896, 2897, 2898, 2899 – and three PTW 23343 Markus – SN 478, 862, 2225 – in the first visit, four PTW 34001 Roos – SN 2896, 2897, 2898, 2899 – and three PTW 23343 Markus – SN 478, 862, 2225 – in the second visit) and three cylindrical ionisation chambers (PTW 31010 Semiflex – SN 4041, 4042, 6361 – in the second visit) were tested and calibrated against the graphite calorimeter. The reference point of the ionisation chambers was taken to be 1 mm inside from the front face of the plane-parallel chambers, whilst for cylindrical chambers, the reference point was taken to be at the central axis of the ionisation chamber. The latter corresponds to the reference point which is positioned at the reference depth in the same way as the chambers are calibrated at NPL.

Figure 3 shows the CCC lateral beam profile (in $x$ and $y$ directions) as well as the sensitive radius/length of the ionisation chambers and the core radius of the calorimeter relative to the centre of the beam. The beam profile measurements were performed with EBT3 radiochromic film at the measurement depth. The dip in the centre region of the beam is due to the presence of the cross-wires in the CCC beam line. The cross-wires are used clinically for beam alignment and are non-removable. Given the smaller radius of the ionisation chambers in comparison with the calorimeter core, a non-uniformity beam profile correction $k_{\mathrm{profile}}$ is applied when calibrating the ionisation chambers against the calorimeter by averaging the lateral beam profiles over the projected diameter/length of the ionisation chambers and correcting it to a similar value over the projected diameter of the calorimeter core (Palmans *et al.* 2004). Ionisation chamber readings are normalised to the readings of the monitor ionisation chamber and were corrected for temperature and pressure, electrometer corrections, polarity and ion recombination. The ion recombination correction factor was derived from a series of experiments by taking ionisation chamber readings $M$ at different polarizing voltages $V$ to obtain a Jaffé plot ($1/M$ against $1/V$), where the saturation charge reading $M_{\mathrm{sat}}$ was obtained by extrapolating $1/V$ to zero by fitting the data points using a quadratic fit (Palmans *et al.* 2006). The ion recombination correction factor $k_{\mathrm{s}}$

was determined by the ratio $k_s = M_{sat}/M_{OV}$, where $M_{OV}$ is the ionisation chamber reading at its operating voltage. Ion recombination was also determined using the two-voltage method (Boag and Currant, 1980) recommended in the IAEA TRS-398 using the quadradic expression.

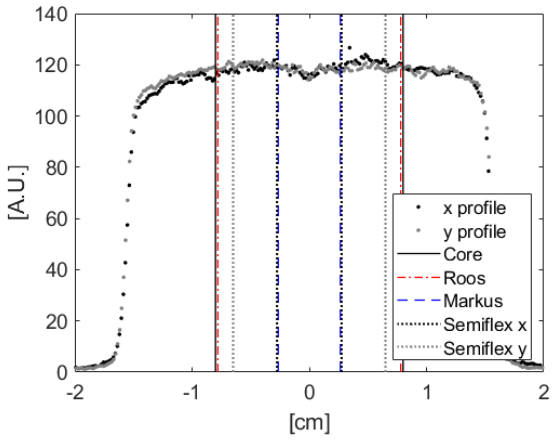


**Figure 3.** CCC lateral beam profile measured with EBT3 radiochromic film at the reference depth for a full-modulated proton beam using a 3 cm collimator. Also plotted is the sensitive diameter of the ionisation chambers used and the calorimeter core relative to the centre of the beam.

The NPL PSPC is used at the user beam quality $Q$ to directly calibrate the ionisation chambers in graphite:

$$N_{D_{g,Q}} = \frac{D_g}{M_g} \qquad (3)$$

where $N_{D_{g,Q}}$ is the absorbed dose-to-graphite calibration coefficient for each ionisation chamber, $D_g$ is the dose in graphite measured by the calorimeter (setup 2) and $M_g$ is the corrected ionisation chamber reading in the graphite phantom (setup 3). Similarly, the absorbed dose-to-water calibration coefficient, $N_{D_{w,Q}}$, is determined by:

$$N_{D_{w,Q}} = \frac{D_g \cdot s_{w,g} \cdot k_{fl}}{M_w} \qquad (4)$$

where $s_{w,g} \cdot k_{fl}$ is the conversion from absorbed dose to graphite in the graphite phantom to absorbed dose to water in the water phantom and $M_w$ is the corrected ionisation chamber reading in the water phantom (setup 1). Four PTW 34001 Roos-type ionisation chambers (SN 2896, 2897, 2898, 2899) are regarded as the transfer standards of the NPL PSPC. These ionisation chambers are calibrated on a regular basis against the NPL PSPC. The absorbed dose to water calibration coefficient, $N^x_{D_{w,Q}}$, for a user ionisation chamber may also be derived by direct comparison of the user ionisation chambers against the NPL reference ionisation chambers:

$$N^x_{D_{w,Q}} = N_{D_{w,Q},ref} \frac{M_{w,ref}}{M_{w,user}} \qquad (5)$$

where $N_{D_{w,Q},ref}$ is the absorbed dose-to-water calibration coefficient for each reference ionisation chamber, $M_{w,ref}$ and $M_{w,user}$ are the corrected ionisation chamber readings at the reference depth in water for the reference and user ionisation chambers, respectively.

The ionisation chambers used in this work were also calibrated in terms of absorbed dose to water in a $^{60}$Co beam at NPL traceable to the UK primary standard of absorbed dose for photon beams. According to the IAEA TRS-398, the determination of absorbed dose to water at the reference depth $z_{ref}$, in a proton beam with a beam quality $Q$ is expressed by:

$$D^{w,TRS-398}_{w,Q} = M_w N_{D_{w,Q_0}} k_Q \qquad (6)$$

where $D^{w,TRS-398}_{w,Q}$ is the dose to water at the reference depth in a water phantom, $M_w$ is the ionisation chamber reading in water, $N_{D_{w,Q_0}}$ is the calibration coefficient in terms of absorbed dose to water in the reference calibration beam quality $Q_0$ and $k_Q$ is the beam quality correction factor that corrects for the difference between

the ionisation chamber response in the beam quality $Q_0$ and that in the user beam quality $Q$. The dose from IAEA TRS-398 was compared with the dose determined following recommendations of the upcoming IPEM Code of Practice which will utilise the NPL PSPC:

$$D_{w,Q}^{w,cal} = D_g \cdot s_{w,g} \cdot k_{fl} \qquad (7)$$

Similarly to equations 6 and 7, which express the quantity absorbed dose to water in a water phantom, absorbed dose to water in a graphite phantom was also determined using equations (8) and (9).

$$D_{w,Q}^{g,cal} = D_g \cdot s_{w,g} \qquad (8)$$

$$D_{w,Q}^{g,chamber} = M_g N_{D_w,Q_0} k_{Q,Q_0} \qquad (9)$$

## 3. Results and Discussion

### *3.1. Correction factors for the NPL PSPC*

Table 1 lists the quantities determined for the NPL PSPC at CCC. To calculate $k_{imp}$, an accurate value of mass for all core components and their properties was considered in the simulations. The thermistors comprise 0.48% of the total mass of the core, the epoxy resin 0.26% and the wires 0.13%. The corrections factors $k_{imp}$, $k_{gap}$, $k_{z,cal}$, $k_{ripple}$ and $k_{fl}$ were found to be close to unity whereas $s_{w,g}$ was largest (1.1202). The $s_{w,g}$ value determined in this work agrees with previous work by Palmans *et al.* (2013) who calculated the water-to-graphite stopping-power ratio for a 60 MeV monoenergetic proton beam, using the FLUKA code and $I$-values from ICRU Report 49 (1993). In their work, for a water-equivalent depth of 1.56 g·cm$^{-2}$, the $s_{w,g}$ was of the order of 1.1190. Its validity in a full-modulated beam is based on the assumption that for a given residual range, the different spectrum of charged-particles between a full-modulated and a monoenergetic beam has a small influence on $s_{w,g}$. ICRU Report 90 (2016) recommends updated $I$-values for water and graphite but it is expected that its influence is negligible on $s_{w,g}$ since they both increased in similar proportion in comparison with ICRU Report 49 (1993) $I$-values. The fluence correction factor $k_{fl}$ (1.0010) is also in agreement with values calculated by Palmans *et al.* (2013) and Lourenço *et al.* (2016).

**Table 1.** Values of the mass of the core, $m_{core,eff}$, the specific heat capacity, $c_{core}$, in function of temperature $T$ in Kelvin, as well as the correction factors determined for the NPL PSPC at CCC.

| | |
|---|---|
| $m_{core,eff}$ (kg) | 0.7536 |
| $c_{core}$ (J.kg$^{-1}$.K$^{-1}$) | 651.567+2.742· ($T$-273.15) |
| $k_{imp}$ | 1.0016 |
| $k_{gap}$ | 1.0008 |
| $k_{z,cal}$ | 1.0000 |
| $k_{ripple}$ | 1.0000 |
| $s_{w,g}$ | 1.1202 |
| $k_{fl}$ | 1.0006 |

Figure 4 shows typical calorimeter runs acquired at CCC. In quasi-adiabatic mode (Figure 4a), the changes in temperature drift of the core, when the irradiation starts and ends, respectively, are clearly visible. In this mode, the energy absorbed in the core is predominantly derived from the measurement of the radiation-induced temperature rise and it is proportional to the specific heat capacity of the core and since no electrical power is dissipated in the core ($\Delta P_{core} = 0$), the main component in equation 2 is the first term. When the calorimeter is operated in isothermal mode, the core is maintained at a constant temperature, thus, during irradiation the electrical power delivered to the core is reduced to keep the core at the same temperature (Figure 4b). In isothermal mode, the energy absorbed is predominantly derived from the difference in electrical power required to maintain the core at a constant temperature before and then during the irradiation. Since there is no temperature change in the core ($\Delta T_{core}$=0), the dominant term in equation 2 is the second one and it is strongly dependent on the mass of the core. In an ideal system, a calorimeter run in isothermal mode (figure 4(b)) would be represented by a square wave. However, there is a transient at the start and end of the run which is due to a slight lag in the response of the feedback loop between the sensing and heating

thermistors. The maximum rate of heating has been adjusted to be the inverse of the maximum rate of cooling hence the transients are symmetrical and cancel each other out (figure 4b).

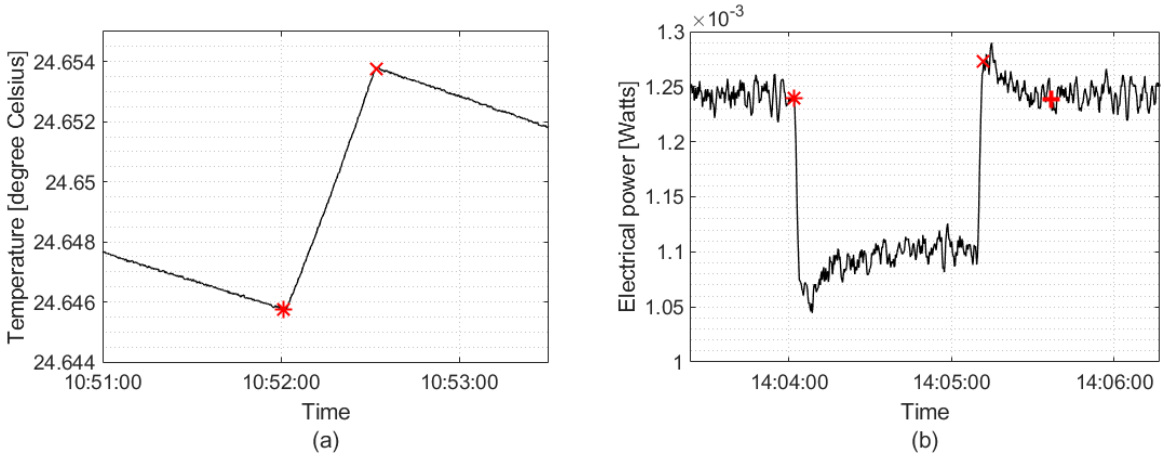


**Figure 4.** Example of calorimeter runs in (a) quasi-adiabatic and (b) isothermal modes at CCC. The star symbol (*) marks the start of the irradiation and the cross symbol (x) marks the end of irradiation. In isothermal mode (c), the positive symbol (+) marks where the electrical powers return to a steady state and data up to this point are considered for analysis.

In this work, the calorimeter was operated using both modes on the same day. Figure 5 shows the ratio of dose measured by the calorimeter in quasi-adiabatic and in isothermal mode throughout the different days/years. The ratio between the two modes was consistent throughout the different datasets with a mean value of 0.990 where the measured dose from isothermal mode was larger than the dose from quasi-adiabatic mode. The calorimeter was built with a PCB positioned around the outer circumference of the inner jacket which could influence the energy measured when the calorimeter is operated in quasi-adiabatic mode and an associated uncertainty is included in the uncertainty budget to account for this possible component (section 3.5.). Transient effects at the start and end of irradiation during isothermal runs could also contribute to this difference (figure 4b). An average dose value between the two modes is reported with an associated uncertainty (section 3.5.). The average dose measured by the NPL PSPC was compared with the dose measured by the NPL primary-standard photon calorimeter in a $^{60}$Co beam, and 6 MV and 10 MV x-ray beams at the NPL, and both calorimeters agreed within the measurement uncertainties across these different beam modalities. Note that the primary-standard photon calorimeter is the basis of NPL contributions to key comparisons undertaken by the International Bureau of Weights and Measures (BIPM) (Picard *et al.* 2015, Kessler *et al.* 2019) and for simplification, the average dose of the two modes is shown in the following figures 7-10.

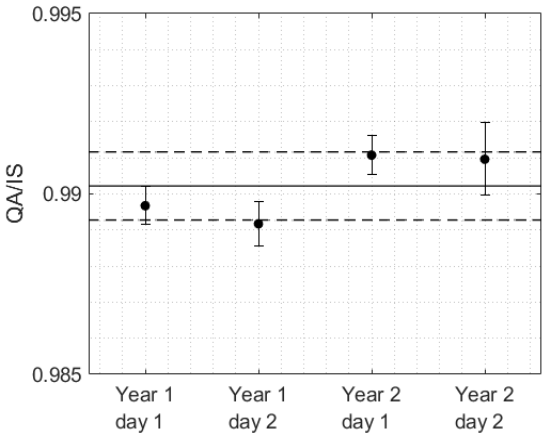


**Figure 5.** Ratio of dose measured by the NPL PSPC in quasi-adiabatic and isothermal mode. The error bars represent type A standard uncertainties. The straight line represents the mean of the ratio (0.9902) and the dashed line its respective standard deviation (0.10%).

*3.2. Correction factors for the ionisation chambers*

The ionisation chambers used in this work are listed in table 2 as well as their respective operating voltage, beam quality correction factors from the IAEA TRS-398 and values for $k_{\text{profile}}$. NPL plane-parallel chambers

are operated at -100 V (collecting electrode is positive with respect to the polarising electrode hence negative charge is collected) while CCC ionisation chambers are operated at +300 V (collecting electrode negative with respect to the polarising electrode hence positive charge is collected). The $k_{\text{profile}}$ is unity for the PTW 34001 Roos because its diameter is similar to that of the NPL PSPC core (figure 3).

**Table 2**. Ionisation chambers used in this work and their respective operating voltages, beam quality correction factors from IAEA TRS-398 ($k_{Q,Q_0}$) and derived non-uniformity beam profile correction $k_{\text{profile}}$.

| Ionisation chambers | Operating voltage (V) | $k_{Q,Q_0}$ for $R_{\text{res}}$=1.56 g·cm$^{-2}$ (IAEA TRS-398) | $k_{\text{profile}}$ |
|---|---|---|---|
| PTW 34001 Roos SN711 (NPL) | -100 | 1.002 | 1.000 |
| PTW 34001 Roos SN1684 (NPL) | -100 | 1.002 | 1.000 |
| PTW 34001 Roos SN2896 (NPL) | -100 | 1.002 | 1.000 |
| PTW 34001 Roos SN2897 (NPL) | -100 | 1.002 | 1.000 |
| PTW 34001 Roos SN2898 (NPL) | -100 | 1.002 | 1.000 |
| PTW 34001 Roos SN2899 (NPL) | -100 | 1.002 | 1.000 |
| PTW 23343 Markus SN478 (NPL) | -100 | 1.003 | 1.011 |
| PTW 23343 Markus SN862 (CCC) | +300 | 1.003 | 1.011 |
| PTW 23343 Markus SN2225 (NPL) | -100 | 1.003 | 1.011 |
| PTW 31010 Semiflex SN4041 (NPL)[a] | +400 | 1.029 | 1.005 |
| PTW 31010 Semiflex SN4042 (NPL)[a] | +400 | 1.029 | 1.005 |
| PTW 31010 Semiflex SN6361 (CCC)[a] | +300 | 1.029 | 1.005 |

[a]Assumed to be equivalent to the PTW Flexible 31002 in IAEA TRS-398 which corresponds to an earlier design of the PTW Semiflex 31010.

Figure 4 shows the Jaffé plots obtained for a PTW 34001 Roos, a PTW 23343 Markus and a PTW 31010 Semiflex ionisation chambers in a proton beam and for a PTW 34001 Roos in a $^{60}$Co beam. A quadratic fit was applied to the data as both beams can be regarded as continuous beams in relation to ion recombination (Palmans *et al.* 2006). Data points at higher voltages (in grey) were not included to find the quadratic fit as the latter should only consider data points for which no charge multiplication occurs (Rossomme *et al.* 2021). Table 3 gives values of the ion recombination correction factor using the experimental data from figure 6, the two-voltage method (Boag and Currant, 1980) recommended in the IAEA TRS-398 (quadratic expression) and a linear fit used at NPL to determine ion recombination corrections in a $^{60}$Co beam. The method based on the extrapolation of the measured data by a quadratic fit (Jaffé plots, figure 6) is very sensitive to fluctuations of the data points. On the other hand, the two-voltage method for continuous beams underestimates the recombination correction (by between 0.1% and 0.4% depending on the ionisation chamber type) because the effect of initial recombination is not included in the model. The two-voltage method is derived from Boag theory for volume recombination (Boag, 1950) and assumes that, if initial recombination is negligible, the inverse of the charge varies linearly with the inverse square of the polarizing voltage for continuous beams. Therefore, an ion recombination correction factor can be derived from measurements at two polarizing voltages. Palmans *et al.* (2006) have done a very extensive and complete analysis of ion recombination corrections for plane-parallel chambers at CCC using data collected at different dose rates and polarizing voltages. As with our findings, the authors reported that the two-voltage method for continuous beams (IAEA TRS-398, 2000) slightly underestimates the ion recombination correction because the effect of initial recombination is not properly dealt with, which can amount to a contribution of 0.3% in proton beams at electric field strengths of 50 V/mm (Palmans *et al.* 2006). The method used at NPL for a $^{60}$Co beam assumes a linear dependence of $1/M$ on $1/V$ to estimate the saturation charge. As can been seen in figure 6(d) for measurements in a $^{60}$Co beam, the quadratic contribution to the fit (volume recombination) is very small and a linear fit (accounting for initial recombination) is a better representation of the data. In the analysis of the data, ion recombination corrections in the proton beam were based on the extrapolation of the measured data by a quadratic fit (Jaffé plots, table 3), while in the $^{60}$Co beam, ion recombination corrections were based on the extrapolation of the data by a linear fit (NPL - linear fit, table 3).

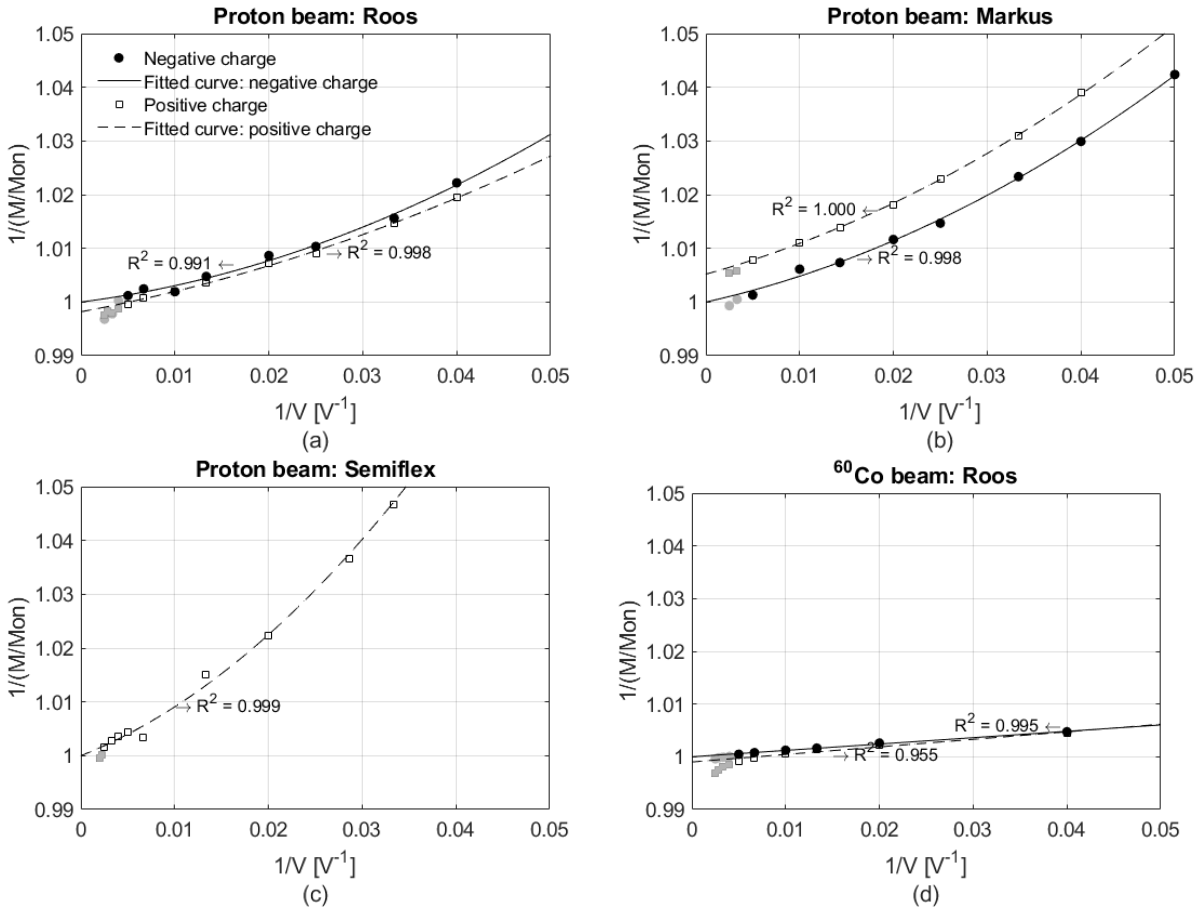


**Figure 6.** Experimental data for the different ionisation chamber types tested. (a), (b), (c) and (d) show the inverse of the charge plotted against the inverse of the polarizing voltage with a quadratic fit in a proton beam and in a $^{60}$Co beam, respectively. The grey values in the plots show the experimental data that were not included in the fit.

**Table 3.** Comparison of numerical values for the recombination correction factors obtained using different methods and different beam modalities.

| | | Proton beam | | $^{60}$Co beam | | |
|---|---|---|---|---|---|---|
| Ionisation chambers | Operating voltage (V) | Jaffé plots Figure 6 | Two-voltage quadratic expression | Jaffé plots Figure 6 | Two-voltage quadratic expression | NPL - Linear fit |
| PTW 34001 Roos | -100 | 1.0031 | 1.0014 | 1.0012 | 1.0002 | 1.0012 |
| PTW 34001 Roos | +100 | 1.0038 | 1.0012 | 1.0014 | 1.0003 | 1.0013 |
| PTW 23343 Markus | -100 | 1.0048 | 1.0016 | N/A | 1.0006 | 1.0030 |
| PTW 23343 Markus | +100 | 1.0057 | 1.0018 | N/A | 1.0006 | 1.0030 |
| PTW 23343 Markus | -300 | 1.0014 | 1.0004 | N/A | 1.0004 | 1.0011 |
| PTW 23343 Markus | +300 | 1.0017 | 1.0005 | N/A | 1.0004 | 1.0011 |
| PTW 31010 Semiflex | +300 | 1.0025 | 1.0008 | N/A | 1.0008 | 1.0033 |
| PTW 31010 Semiflex | +400 | 1.0019 | 1.0003 | N/A | 1.0004 | 1.0019 |

*3.3. Consistency of the NPL PSPC with respect to ionisation chambers over time*

Figure 7 represents the absorbed dose calibration coefficients determined at CCC for those ionisation chambers that were calibrated throughout different days/years against the NPL PSPC (equations 3 and 4). The error bars represent a type A standard uncertainty of 0.3% as this is the threshold of action considered at NPL for variations in the absorbed dose photon calibration coefficients for the same ionisation chamber calibrated at different days or years. The calibration coefficients in water and graphite for the PTW 34001 Roos chambers were all within 0.3%. For the three PTW 23343 Markus-type chambers tested, the calibration coefficients resulting from consecutive calibration campaigns agreed within the uncertainties for two of the chambers. The third chamber showed greater variation but it was subsequently discovered to have a significant leakage current and was therefore discounted from the reported results in the subsequent figures. Figure 7(c) also shows the $N_{D_{w,Q}}^{x}$ coefficients for the user ionisation chambers calculated using equation (5),

where $N_{D_{w,Q}}^{x}$ was found by considering an average between the values derived from the four reference PTW 34001 Roos ionisation chambers (standard deviation <0.01%). Excellent agreement was found between the $N_{\mathrm{D_{w,Q}}}$ coefficients derived by direct comparison of the user ionisation chambers against the NPL PSPC (equation 4) and $N_{D_{w,Q}}^{x}$ derived by direct comparison of the user ionisation chambers against the NPL reference ionisation chambers (equation 9). The long-term stability of the PTW 34001 Roos ionisation chambers reported by Bass *et al.* (2009) for electron beams and the results from this work support the use of this type of ionisation chamber as reference and transfer standards for protons beam.

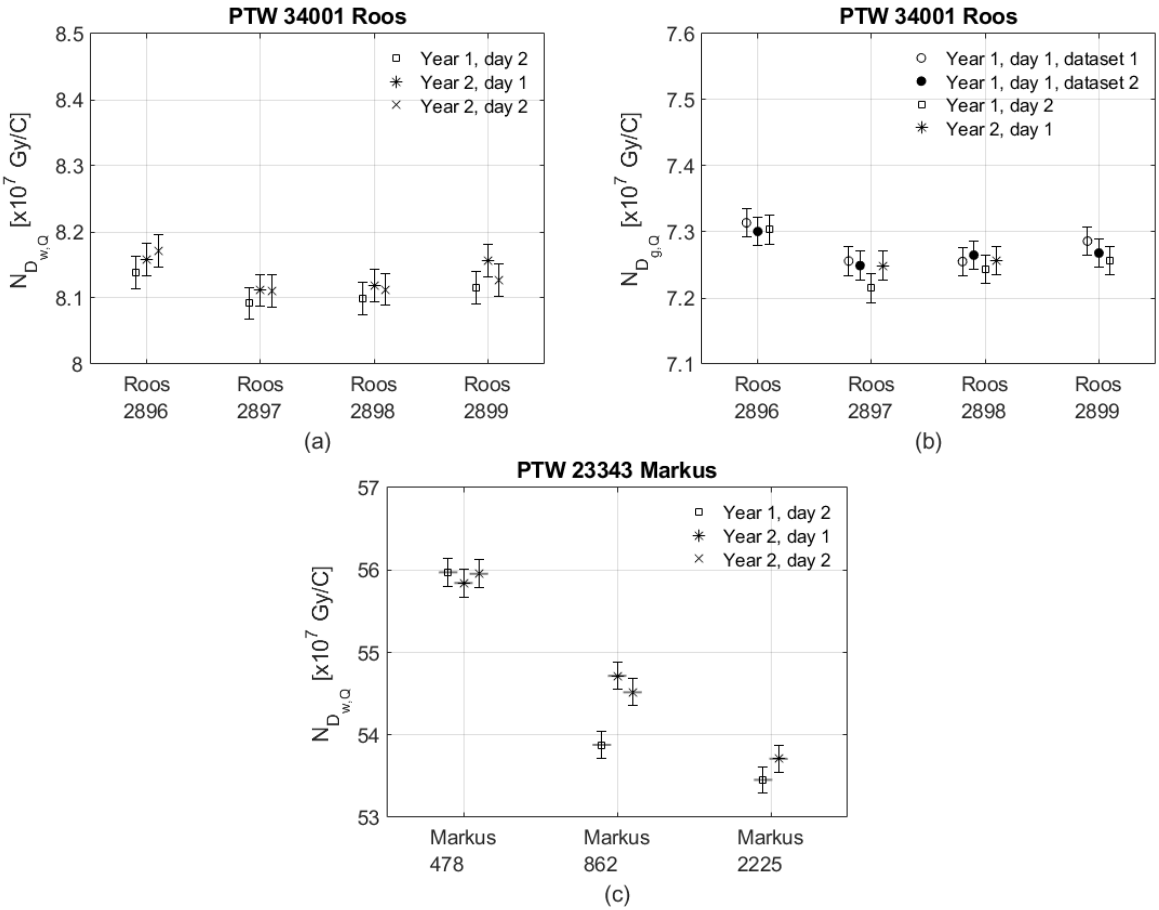


**Figure 7.** The symbols represent the absorbed dose calibration coefficients determined at CCC by direct comparison against the NPL PSPC: (a) and (b) for the PTW 34001 Roos type chambers in water and graphite, respectively, and (c) for the PTW 23343 Markus type chambers in water. The straight lines (shown in (c) only) represent the absorbed dose calibration coefficients determined for the user ionisation chambers by direct comparison against the NPL reference ionisation chambers. The error bars represent type A standard uncertainties.

*3.4. Comparison between the dose determined by the NPL PSPC and that derived from $^{60}$Co calibrated ionisation chambers using IAEA TRS 398*

Figure 8 shows the ratio between the absorbed dose to water measured by the NPL PSPC (equation 7) following recommendations of the upcoming IPEM Code of Practice and the absorbed dose to water derived from ionisation chambers (equation 6) applying the IAEA TRS-398 protocol. There is a consistent difference for each ionisation chamber type between the dose from the NPL PSPC and the dose derived from the IAEA TRS-398. The dashed line represents the mean values of the ratio: 0.982 for the PTW 34001 Roos type chambers, 0.997 for the PTW 23343 Markus type chambers and 1.002 for the PTW 31010 Semiflex. These results are in agreement with the results from Palmans *et al.* (2004) where a ratio of 0.996 was found for the PTW 23343 Markus type chambers between the dose measured using a small-body portable calorimeter and the dose determined from ionisation chambers applying the IAEA TRS-398 protocol at CCC in a modulated beam. Although the differences found between the dose reported from the two protocols appear large, the maximum difference found lies within the associated measurement uncertainties of the protocols with the new procedure based on the NPL PSPC giving a significant improvement in uncertainty in comparison with the IAEA TRS-398 protocol (section 3.5.). The results from figure 8 suggest that the $k_Q$ factors reported in the IAEA TRS-398

protocol should be revised as they correspond to the largest source of uncertainty, 1.7% (1$\sigma$) for cylindrical chambers and 2.1% (1$\sigma$) for plane-parallel chambers. These factors were determined analytically, where ionisation chamber-specific perturbation factors in proton beams were assumed to be unity. Lourenço *et al.* (2019) determined ionisation chamber-specific perturbation factors for plane-parallel chambers in proton beams numerically, using Monte Carlo simulations. Their results showed that when nuclear interactions were discarded, ionisation chamber-specific perturbation factors were close to unity as suggested by the IAEA TRS-398 protocol. Importantly however, they also showed that when all charged particles were transported, ionisation chamber-specific perturbation factors could amount up to 1%.

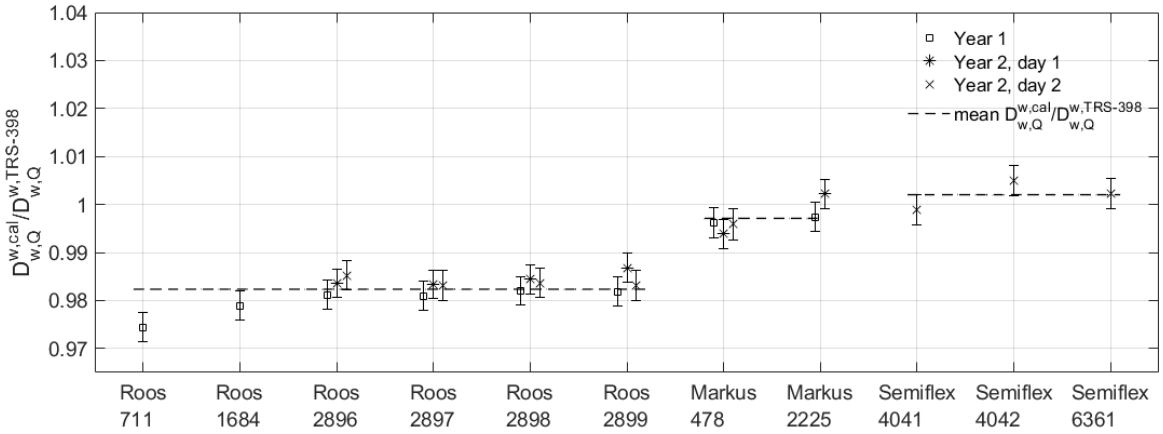


**Figure 8.** Ratio between the dose-to-water in a water phantom determined by the NPL PSPC following recommendations of the upcoming IPEM Code of Practice and by ionisation chambers following recommendations of IAEA TRS-398 protocol. The dashed line represents the mean values for each ionisation chamber type. The error bars represent type A standard uncertainties.

In recent years, several Monte Carlo based studies have determined $k_Q$ factors numerically for proton beams (Gomà *et al.* 2016, Gomà and Sterpin *et al.* 2019, Baumann *et al.* 2020 and 2021 and Kretschmer *et al.* 2020) using detailed modelling of ionisation chambers. Figure 9 shows $k_Q$ factors experimentally determined in this work, using the NPL PSPC, in comparison with $k_Q$ factors analytically derived from the IAEA TRS-398 protocol and numerically calculated from the aforementioned Monte Carlo studies. The $k_Q$ factors from this work shown in figure 9 represent a mean value of all ionisation chambers of each type tested: 0.991 for the PTW 34001 Roos type, 1.006 for the PTW 23343 Markus type chambers and 1.038 for the PTW 31010 Semiflex. Note that $k_{Q,Q_0}$ factors derived analytically and numerically are strongly dependent on the mean energy needed to create an ion pair in air between the beam qualities $Q$ and $Q_0$, $W_{\mathrm{air},Q}/W_{\mathrm{air},Q_0}$. In the IAEA TRS-398 protocol, $W_{\mathrm{air},Q}/W_{\mathrm{air},Q_0}$ is taken as 1.008, while the recent Monte Carlo studies considered 1.014 as recommended by the ICRU Report 90 (2016). Although the existing Monte Carlo data only includes calculations of $k_Q$ factors for a residual range larger than 2 g·cm$^2$, their trend suggests that the $k_Q$ factors experimentally measured in this work agree within uncertainties, with the Monte Carlo derived factors. For the PTW 34001 Roos type chambers, numerically and experimentally determined $k_Q$ factors are below the recommended values from IAEA TRS-398 by up to 1.5% while for the PTW 23343 Markus chamber is found to be in excellent agreement. Currently, there is no numerical data reported for the PTW 31010 Semiflex type chamber.

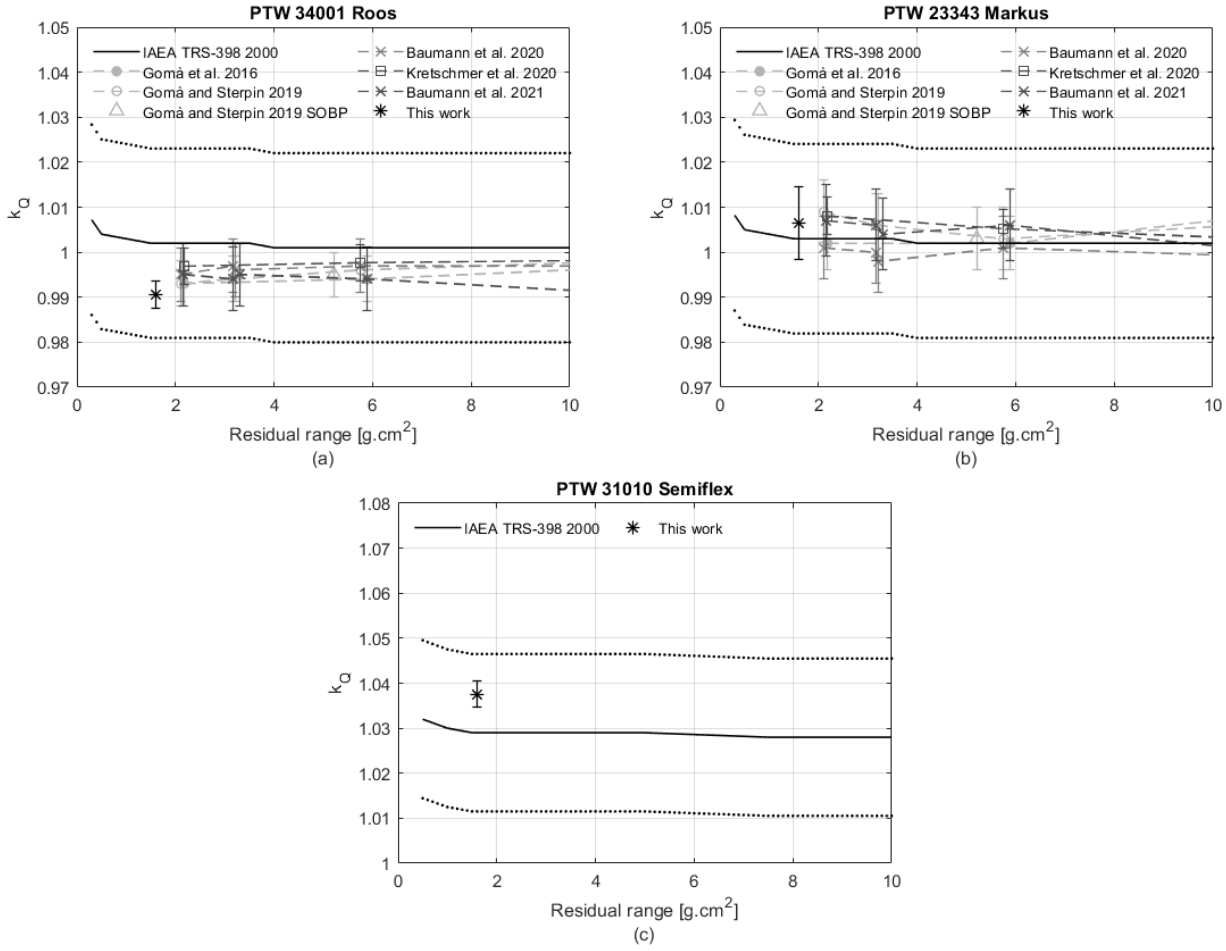


**Figure 9.** Comparison of $k_Q$ factors determined analytically (straight line), numerically (connected symbols with a dashed line) and experimentally (stars) in function of the residual range. The error bars and dotted lines represent one standard type A uncertainty in the data points and IAEA TRS-398 values, respectively.

Similar to figure 8, figure 10 represents the ratio between the absorbed dose to water in a graphite phantom determined using the NPL PSPC (equation 8) and ionisation chambers applying IAEA TRS-398 (equation 9) for the ionisation chambers tested in the graphite phantom (setup 3). For the four PTW 34001 transfer Roos chambers, the mean value of the ratio was 0.986 when considering absorbed dose to water in a graphite phantom (figure 10) whereas for the same four PTW 34001 transfer Roos chambers the mean value of the ratio was 0.983 when considering absorbed dose to water in a water phantom (figure 9). The good agreement between these ratios supports the fluence correction factor used to convert from dose to graphite to dose to water determined in this work, using Monte Carlo simulations (table 1).

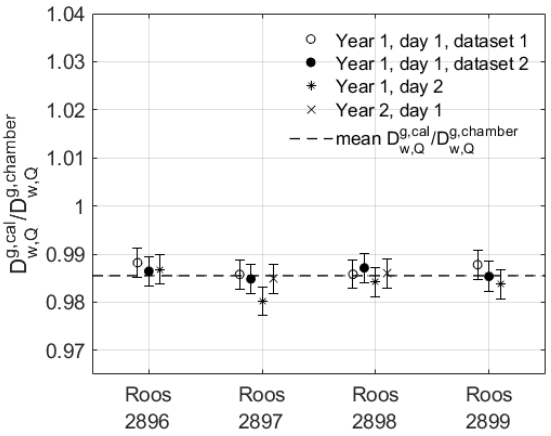


**Figure 10.** Ratio between the dose-to-water in a graphite phantom determined by the NPL PSPC following recommendations of the upcoming IPEM Code of Practice and by ionisation chambers following recommendations of IAEA TRS-398 protocol. The dashed line represents the mean value. The error bars represent type A standard uncertainties.

### 3.5. Uncertainties

The sources of uncertainties for determining $D_{w,Q}^{w,cal}$ and $N_{D_{w,Q}}$ are presented in table 4 and 5 respectively. All uncertainties are expressed as relative uncertainties and were calculated in accordance with the *Guide to the Expression of Uncertainty in Measurement* (JCGM 2008). The overall uncertainty is quoted to $1\sigma$ and $2\sigma$.

**Table 4.** Relative uncertainty of absorbed dose to water at the reference depth in water, $D_{w,Q}^{w,cal}$.

| Sources of uncertainties (%) | Type A | Type B |
|---|---|---|
| Calorimeter corrections | | |
| Graphite mass and impurities | <0.01 | 0.09 |
| Core alignment on beam axis | - | <0.01 |
| Reference depth | 0.06 | 0.12 |
| $k_{z,cal}$ | - | 0.10 |
| $k_{ripple}$ | - | 0.01 |
| Monte Carlo corrections | | |
| $k_{imp}.k_{gap}$ | 0.11 | 0.12 |
| $s_{w,g}.k_{fl}$ | 0.02 | 0.42 |
| Electrical calibrations | 0.20 | 0.06 |
| Specific heat capacity of the core | 0.08 | 0.26 |
| PCB | - | 0.25 |
| Calorimeter measurements | | |
| Repeatability in quasi-adiabatic mode | 0.06 | |
| Repeatability in isothermal mode | 0.06 | |
| Average quasi-adiabatic and isothermal modes | - | 0.40 |
| Total | 0.26 | 0.72 |
| Overall ($1\sigma$) | 0.77 | |
| Overall ($2\sigma$) | 1.53 | |

**Table 5.** Relative uncertainty of the absorbed dose-to-water calibration coefficient at the reference depth in water, $N_{D_{w,Q}}$.

| Sources of uncertainties (%) | Type A | Type B |
|---|---|---|
| $D_{w,Q}^{w,cal}$ | 0.26 | 0.72 |
| Ionisation chambers repeatability | 0.03 | - |
| Electrometer calibration | - | 0.10 |
| Electrometer leakage correction | - | 0.05 |
| Ion recombination correction | | 0.03 |
| Polarity correction | - | 0.03 |
| $k_{z,chamber}$ | - | 0.10 |
| $k_{an,chamber}$ | - | 0.35 |
| $k_{profile}$ | - | 0.20 |
| Air temperature | - | 0.06 |
| Air pressure | - | 0.05 |
| Relative humidity | - | 0.10 |
| Total | 0.26 | 0.81 |
| Overall ($1\sigma$) | 0.89 | |
| Overall ($2\sigma$) | 1.78 | |

The overall uncertainty of $D_{w,Q}^{w,cal}$ includes uncertainties for the physical dimensions of the calorimeter and its positioning at the reference depth, Monte Carlo correction factor uncertainties, electrical calibrations of the instrumentation used to measure the calorimeter output, measurement of the specific heat capacity of the calorimeter core, presence of the PCB and uncertainties related with the calorimeter measurements. The overall uncertainty is dominated by the uncertainty of the conversion from dose to graphite to dose to water (0.42%), the uncertainty of averaging the dose between the two modes of operation (0.40%), value of the specific heat capacity of the core (0.27%) and for any possible effect due to the presence of the PCB (0.25%).

The conversion from dose to graphite to dose to water is largely dependent on the choice of the $I$-values for water and graphite that directly influence the water-to-graphite stopping power ratio. The $I$-values enter logarithmically into the stopping power equation, thus, for the clinical energy range, the relative change of the stopping power is smaller than the respective relative change on the $I$-value. In this work, the recommended $I$-values for water and graphite from ICRU Report 90 (2016) were used, $78\pm2$ eV and $81\pm1.8$ eV, respectively,

and to estimate the associated uncertainty on the dose conversion correction, Monte Carlo simulations were performed using different $I$-values for water and graphite; the latter chosen to be within their stated uncertainty. Palmans *et al.* (2004) used a relative standard uncertainty of 1% for the water-to-graphite stopping power ratio based on estimates from the IAEA TRS-398 and ICRU Report 49 (1993). The $I$-values for water and graphite both increased almost proportionally in ICRU Report 90 (2016) in comparison with the values from ICRU Report 49 (1993), which results in minor changes to the water-to-graphite stopping power ratio. However, the associated uncertainty on the $I$-values decreased considerably, from 4.0% to 2.6% for water and from 5.1% to 2.2% for graphite, which leads to a significant decrease in the associated uncertainty on the water-to-graphite stopping power ratio. Each dataset of calorimeter measurements is comprised of at least 20 calorimeter runs for each mode of operation and an average dose value between the two modes of operation is then taken as our best estimate of the true value of absorbed dose to water. The associated uncertainty of the dose averaging from the two modes of operation was determined assuming a triangular distribution with full-width at half maximum (FWHM) the difference between the two measured values. The value of specific heat capacity of graphite is readily available from the literature, however, in an attempt to minimise the contribution to the uncertainty budget, a sample of graphite from the same block of material used to manufacture the NPL PSPC was tested at NPL, and the specific heat capacity measured experimentally. The uncertainty reported is associated with the experimental apparatus (Williams *et al.* 1993). The fourth largest component in the uncertainty budget is associated with the PCB which is positioned radially around the centre-line of the core. A series of tests were carried out using radiation-absorbing brass masks to shield the core and/or the surrounding PCB from the incoming beam of radiation. These tests involved a series of irradiations over timeframes ranging from tenths of seconds to several minutes to ascertain how radiation absorbed by the PCB may impact the measurement of dose to the core. The results obtained showed no detectable impact beyond the random uncertainty of the dose measured by the core, therefore, a pragmatic approach has been taken and a PCB component has been included in the uncertainty budget. Future designs of the calorimeter will not position a PCB in such close proximity to the core or within the radiation field area, thus eliminating this source of uncertainty.

The overall uncertainty of $N_{D_{\mathrm{w},Q}}$ comprises of the repeatability of the ionisation chamber measurements and uncertainties associated with the electrometer, ion recombination and polarity corrections as well as positioning and beam dependent uncertainties. One of the largest sources of uncertainty is due to the correction factor for the axial non-uniformity of the proton beam (ripple) over the ionisation chamber in the water phantom - $u(k_{\mathrm{an,chamber}})$ (table 5). This uncertainty is larger for plane-parallel than cylindrical chambers because protons that enter a cylindrical chamber have different equivalent depths and there is some averaging effect as in the calorimeter. For example, the calorimeter core is 2 mm thick which is equivalent to 3 mm water-equivalent thickness. At the CCC, the ripple spacing is about 1 mm hence the dose is averaged over 3 periods of the ripple and, consequently, less dependent on its position – $u\left(k_{\mathrm{ripple}}\right) = 0.01\%$ (table 4). In a plane-parallel chamber, protons that enter the ionisation chamber have the same water equivalent depth, and the dose is regarded as being sampled at a point. In consequence, positioning uncertainties have a larger contribution, and an 0.35% uncertainty is assigned to account for this.

This gives an overall uncertainty in $D_{\mathrm{w},Q}^{\mathrm{w,cal}}$ of 0.77% at the 68% confidence level ($1\sigma$) and $N_{D_{\mathrm{w},Q}}$ as supplied to the user of 0.89% at the 68% confidence level ($1\sigma$). Note that uncertainties are reported at $2\sigma$ level in calibration certificates provided by NPL. This corresponds to a significant improvement on the confidence in dose delivered in proton beams in comparison with the IAEA TRS-398 protocol (2000) which gives an overall uncertainty in $D_{\mathrm{w},Q}^{\mathrm{w,TRS-398}}$ of 2.0% and 2.3% at the 68% confidence level ($1\sigma$) for cylindrical and plane-parallel chambers, respectively.

## 4. Conclusions

In this work, user and NPL reference ionisation chambers were calibrated in terms of absorbed dose to water following the recommendations of the upcoming IPEM Code of Practice for proton therapy dosimetry as well as according to the existing IAEA TRS-398 protocol in a low-energy passively scattered proton beam. Differences between the two protocols were found but fell within the uncertainties determined according to IAEA TRS-398 protocol. The measurement uncertainty from calibrations directly traceable to the NPL PSPC in the user clinical proton beam are at least half of those reported using the traditional IAEA TRS-398/$^{60}$Co calibration based route (currently with an uncertainty ≥2.0% at 68% confidence level) thus ensuring significantly more confidence in the dose delivered. As the number of proton therapy centres continues to grow it becomes more important that the dose is delivered consistently between them and so reduce the variability in dose delivery, and ultimately to the patient population.

The upcoming IPEM Code of Practice for reference dosimetry of proton beams will utilise the NPL PSPC and it will enable the provision of a direct absorbed dose to water calibration service for proton therapy beams. The NPL PSPC has previously been validated by comparison in a $^{60}$Co beam, a 6 and 10 MV photon beam with the UK primary standard graphite calorimeter for photon beams, which is included in the international key comparison database held by BIPM. The establishment of a purpose built primary standard for the determination of absorbed dose in proton beams, combined with the introduction of a calibration service will reduce the uncertainty in dose delivered to patients, ensuring optimal tumour control and improve accuracy in proton therapy treatments, both within and between treatment facilities, and establish consistent standards that underpin the development of clinical trials.

**Acknowledgements**

The authors would like to thank all the past and present members of the Medical Radiation Science and Physics Groups at NPL who contributed to the development and commissioning of the NPL PSPC and the cyclotron staff at the Clatterbridge Cancer Centre (UK) for their assistance during the experiments. The authors acknowledge the use of the UCL Myriad High Performance Computing Facility (Myriad@UCL), and associated support services, in the completion of this work, and the FLUKA mailing list for all the support with FLUKA code.

**References**

Andreo P, Burns D T, Hohlfeld K, Huq M S, Kanai T, Laitano F, Smyth V G, Vynckier S 2000 Absorbed dose determination in external beam radiotherapy: an international code of practice for dosimetry based on standards of absorbed dose to water IAEA *Technical Report Series 398* (Vienna: IAEA)

Baker C, Shipley D, Palmans H and Kacperek A 2006 Monte Carlo modelling of a clinical proton beam-line for the treatment of ocular tumours *Nucl. Instrum. Methods Phys. Res.* A **562** 1005–1008

Bass G, Thomas R and Pearce J 2009 The calibration of parallel-plate electron ionisation chambers at NPL for use with the IPEM 2003 code of practice: summary data *Phys. Med. Biol.* 54 N115–N124

Baumann KS, Kaupa S, Bach C, Engenhart-Cabillic and Zink K 2020 Monte Carlo calculation of beam quality correction factors in proton beams using TOPAS/GEANT4 *Phys. Med. Biol.* **65** 055015

Baumann KS, Derksen L, Witt M, Burg JM, Engenhart-Cabillic R and Zink K 2021 Monte Carlo calculation of beam quality correction factors in proton beams using FLUKA *Phys. Med. Biol.* **65** 17NT01

Böhlen T T, Cerutti F, Chin M P W, Fassò A, Ferrari A, Ortega P G, Mairani A, Sala P R, Smirnov G and Vlachoudis V 2014 The FLUKA code: developments and challenges for high energy and medical applications *Nucl. Data Sheets* **120** 211–214

Bonnett D E, Kacperek A, Sheen M A, Goodall R and Saxton T E 1993 The 62 MeV proton beam for treatment of ocular melanoma at Clatterbridge *Br. J. Radiol.* **66** 907–14

Delacroix S, Bridier A, Mazal A, Daures J, Ostrowsky A, Nauraye C, Kacperek A, Vynkier S, Brassard N and Habrand J L 1997 Proton dosimetry comparison involving ionometry and calorimetry *Int J Radiat Oncol Biol Phys* **37**(3) 711-718

Ferrari A, Sala P R, Fassò A and Ranft J 2005 FLUKA: a multi-particle transport code CERN-2005–10, INFN/TC_05/11, SLAC-R-773

Gagnebin S, Twerenbold D, Pedroni E, Meer D, Zenklusen S and Bula C 2010 Experimental determination of the absorbed dose to water in a scanned proton beam using a water calorimeter and an ionisation chamber *Nucl. Instrum. Methods Phys. Res. B* **268** 524–8

Green S, Amos R, Van den Heuvel F, Kacperek A, MacKay R I, Palmans H, D'Souza D and Thomas R 2017 IPEM Code of Practice for proton and ion beam dosimetry: update on work in progress *Radiotherapy and Oncology* **123** S783-S784

Gomà C, Andreo P and Sempau J 2016 Monte Carlo calculation of beam quality correction factors in proton beams using detailed simulation of ionisation chambers *Phys. Med. Biol.* **61** 2389–406

Gomà C and Sterpin E. 2019 Monte Carlo calculation of beam quality correction factors in proton beams using PENH *Phys. Med. Biol.* **64** 185009

ICRU Report 24 1976 Determination of Absorbed Dose in a Patient Irradiated by Beams of X or Gamma Rays in Radiotherapy Procedures *ICRU Report No 24* (Bethesda, MD: International Commission on Radiation Units and Measurements)

ICRU Report 49 1993 Stopping Powers and Ranges for Protons and Alpha Particles *ICRU Report No 49* (Bethesda, MD: International Commission on Radiation Units and Measurements)

ICRU Report 78 2008 Prescribing, Recording, and Reporting Proton-Beam Therapy *ICRU Report No 78* (Bethesda, MD: International Commission on Radiation Units and Measurements)

ICRU Report 90 2016 Key Data for Ionizing-Radiation Dosimetry: Measurement Standards and Applications *ICRU Report No 90* (Bethesda, MD: International Commission on Radiation Units and Measurements)

JCGM 2008 Evaluation of measurement data - Guide to the Expression of Uncertainty in Measurement (Joint Committee for Guides in Metrology (JCGM), 1st edition)

Kacperek A 2009 Protontherapy of eye tumours in the UK: a review of treatment at Clatterbridge *Appl. Radiat. Isot.* **67** 378–86

Karger C P, Jäkel O, Palmans H and Kanai Tatsuaki 2010 Dosimetry for ion beam radiotherapy *Phys. Med. Biol.* **55** R193–R234

Kessler C, Burns D T, Kelly M, Maughan D J, Bass G A, Shipley D R, Sander T, Lee N D, Cashmore M and Duane S 2019 Comparison of the standards for absorbed dose to water of the NPL, United Kingdom and the BIPM for $^{60}$Co γ rays *Metrologia* **56** 06008

Kretschmer J, Dulkys A, Brodbek L, Stelljes T S, Looe H K, Poppe B 2020 Monte Carlo simulated beam quality and perturbation correction factors for ionisation chambers in monoenergetic proton beams *Med. Phys.* **47** 11

Lillicrap S C, Owen B, Williams J R, Williams P C 1990 Code of Practice for high-energy photon therapy dosimetry based on the NPL absorbed dose calibration service *Phys Med Biol*. **35** 1355–1360

Medin J 2010 Implementation of water calorimetry in a 180 MeV scanned pulsed proton beam including an experimental determination of *kQ* for a Farmer chamber *Phys. Med. Biol.* **55** 3287-98

Lourenço A, Thomas R, Bouchard H, Kacperek A, Vondracek V, Royle G, Palmans H 2016 Experimental and Monte Carlo studies of fluence corrections for graphite calorimetry in low- and high-energy clinical proton beams *Med. Phys.* **43** 4122-32

Lourenço A, Bouchard H, Galer S, Royle G and Palmans H 2019 The influence of nuclear interactions on ionisation chamber perturbation factors in proton beams: FLUKA simulations supported by a Fano test *Med. Phys.* **46** 885–91

Palmans H, Seuntjens J, Verhaegen F, Denis J-M, Vynckier S, Thierens H 1996 Water calorimetry and ionisation chamber dosimetry in an 85-MeV clinical proton beam *Med. Phys.* **23** 643-50

Palmans H, Thomas R, Simon M, Duane S, Kacperek A, DuSautoy A, Verhaegen F 2004 A small-body portable graphite calorimeter for dosimetry in low-energy clinical proton beams *Phys. Med. Biol.* **49**(16) 3737–3749

Palmans H, Thomas R and Kacperek A 2006 Ion recombination correction in the Clatterbridge Centre of Oncology clinical proton beam *Phys. Med. Biol.* **51** 903-17

Palmans H, Al-Sulaiti1 L, Andreo P, Shipley D, Lühr A, Bassler N, Martinkovič J, Dobrovodský J, Rossomme S, Thomas R A S 2013 Fluence correction factors for graphite calorimetry in a low-energy clinical proton beam: I. Analytical and Monte Carlo simulations *Phys. Med. Biol.* **58** 3481–99

Perl J, Shin J, Schümann J, Faddegon B, Paganetti H 2012 TOPAS: an innovative proton Monte Carlo platform for research and clinical applications *Med. Phys.* **39**(11) 6818-37

Petrie L 2016 Characterisation of a Graphite Calorimeter in Scanned Proton Beams (PhD thesis, University of Surrey, Guildford)

Picard S, Burns D T, Roger P, Duane S, Bass G A, Manning J W and Shipley D R 2015 Key comparison BIPM.RI(I)-K6 of the standards for absorbed dose to water at 5 g cm$^{-2}$ and 7 g cm$^{-2}$ of the NPL, United Kingdom and the BIPM in accelerator photon beams *Metrologia* **52** 06010

Renaud J, Rossomme S, Sarfehnia A, Vynckier S, Palmans H, Kacperek A, Seuntjens J 2016 Development and application of a water calorimeter for the absolute dosimetry of short-range particle beams *Phys. Med. Biol.* **61** 6602

Romano F, Shipley D, Petrie L M, Palmans H 2017 Monte Carlo calculated correction factors for a proton calorimeter in clinical proton beams *Physica Medica* **42** S35-S36

Rossomme S, Lorentini S, Vynckier S, Delor A, Vidal M, Lourenço A, Palmans H 2021 Correction of the measured current of a small-gap plane-parallel ionisation chamber in proton beams in the presence of charge multiplication, *Zeitschrift für Medizinische Physik* (in press)

Sarfehnia A, Clasie B, Chung E, Lu H M, Flanz J, Cascio E, Engelsman M, Paganetti H, Seuntjens J 2010 Direct absorbed dose to water determination based on water calorimetry in scanning proton beam delivery *Med. Phys.* **37** 3541-50

Schulz R J, Verhey L J, Huq M S, Venkataramanan N 1992 Water calorimeter dosimetry for 160 MeV protons *Phys. Med. Biol.* **37** 947-53

Seuntjens J and Duane S 2009 Photon absorbed dose standards *Metrologia* **46**(2) S39

Shipley D, Romano F, Palmans H 2018 Monte Carlo calculated correction factors for a proton calorimeter in clinical proton beams *Radiotherapy and Oncology* **127** S459

Siebers J V, Vatnitsky S M, Miller D W and Moyers M F 1995 Deduction of the air *w* value in a therapeutic proton beam *Phys. Med. Biol.* **40** 1339-56

Thomas R A S, Bolt M A, Bass G, Nutbrown R, Chen T, Nisbet A, Clark C 2017 Radiotherapy reference dose audit in the United Kingdom by the National Physical Laboratory: 20 years of consistency and improvements *Phys. Imaging. Radiat. Oncol.* **3** 21-27

Williams A J, Burns D T and McEwen M 1993 Measurement of the specific heat capacity of the electron-beam graphite calorimeter NPL Report RSA(EXT) **40** (Teddington: National Physical Laboratory)

Verhey L J, Koehler A M, McDonald J C, Goitein M, Ma I-C, Schneider R J, Wagner M 1979 The determination of absorbed dose in a proton beam for purposes of charged-particle radiation therapy *Radiation Research* **79**(1) 34-54